

# Structural and electrical properties of manganese doped cobalt ferrite nanoparticles.

M Z Ahsan<sup>1,2</sup>, F A Khan<sup>2\*</sup>

<sup>1</sup>Department of Physics, Military Institute of Science and Technology (MIST), Dhaka, Bangladesh

<sup>2</sup>Department of Physics, Bangladesh University of Engineering and Technology (BUET), Dhaka, Bangladesh

## Abstract

The structural, electrical and magnetoresistive properties of manganese doped cobalt ferrite nanoparticles have been investigated through measurements of dc and ac magnetic properties. The samples were synthesized *via* standard solid state reaction route. The X-ray diffraction patterns confirm the formation of spinel structure of the synthesized samples. Field Emission Electron Microscopy (FESEM) is done to estimate the average particle size. The energy dispersion spectrum marks the presence of Co, Mn, Fe and O in the studied sample. The dielectric constant and impedance were measured in the frequency range 100 Hz to 120 MHz and temperature range 400°C to 1200°C. Frequency dependent dispersion exhibits an anomalous behavior in the range between 1 MHz and 10 MHz. A pronounced leftward shift of relaxation peaks in the dispersion observed in the loss factor  $\tan\delta$  curve. The fabricated nanoparticles have shown semiconducting behaviour at low frequency regime (100 Hz, 1 kHz and 10 kHz) but a purely insulating behaviour at higher frequency regime (100 kHz and 1 MHz) indicating a second order phase transition. The magnetoresistive properties of  $\text{Co}_{1.125}\text{Mn}_{0.125}\text{Fe}_{1.875}\text{O}_4$  in particular is assumed to be originated from the localized electrons and the magnetoresistance decreases monotonically with increasing magnetic field and hence bears the signature of a semiconducting material. However comparing the transvers and longitudinal magnetoresistance of the material we found that both the magnetoresistive parameters are magnetic field dependent and thus presumed to be a signature of mixed metallic and semiconducting nature of the material.

**Keywords:** Cobalt ferrite, dielectric constant, ac conductivity, dielectric relaxation, magnetoresistance.

Accepted on August 16, 2018

## Introduction

Cobalt ferrites are hard ferrite materials because of their excellent chemical stability, mechanical hardness, reasonable saturation magnetization and high magneto crystalline anisotropy [1]. They are now being used in high-density recording media, ferro-fluids, Magnetic Resonance Imaging (MRI), biomedical diagnostics, radio frequency hyperthermia and drug delivery etc. Nanocrystalline cobalt ferrites are also the potential candidates for the fabrication of microwave components, memories, capacitors, and filter design as reported elsewhere in literatures [1-6]. It is of inverse spinel structure where relatively larger oxygen ions ( $\text{O}^{2-}$ ) form cubic closed pack (ccp) lattice. Its tetrahedral (A) and octahedral (B) sites formed by the oxygen ions ( $\text{O}^{2-}$ ) are occupied by metal ions ( $\text{Fe}^{3+}$  and  $\text{Co}^{2+}$  ions). A site is occupied by  $\text{Fe}^{3+}$  ions and the B site by  $\text{Fe}^{3+}$  and  $\text{Co}^{2+}$  ions in equal proportionate [7]. Earlier studies show that cobalt ferrites doped with metallic ions have received renewed attention among the researchers to optimize them both for sensor and high frequency applications. These applications are mostly based on their structural, magnetic and electrical properties and their tailoring the substitution level of the dopants, sintering temperature, and their particle size [7]. Accordingly efforts have already been made to substitute Co or Fe by metal ions for changing the structural, magnetic and electrical properties in a controlled manner as reported in various literatures. Cobalt

ferrite is a magnetic semiconductor, where  $\text{Fe}^{2+}$  and  $\text{Co}^{2+}$  ions refer to the n-type and p-type carriers respectively. These carriers are localized and isolated from each other and leading to hopping mechanism of charge transport between metal ions of different valences at crystallographically equivalent lattice points as reported in literature [8]. So, substitution of Mn in cobalt ferrite system both in stoichiometric and non-stoichiometric compositions may have the ability to control Co/Fe ratio and thus may change the electrical properties of the system under the influence of ac field and temperature variation. In the recent past it is reported that the conductivity in Sn substituted  $\text{CoFe}_2\text{O}_4$  ferrites is predominantly due to the intrinsic bulk grains at room temperature. However with increasing temperature evolution of grain boundary conduction has been appeared to have occurred [9]. The dielectric dispersion is rapid at lower frequency region and remains almost independent at the higher frequency region. The inclusion of Zn into the  $\text{CoZn}_x\text{Fe}_{2-x}\text{O}_4$  has no pronounced effect on the dielectric constant at higher frequency, but significantly decreases at the lower frequency range as reported earlier [10]. The frequency and temperature dependent dielectric constants indicate that pure  $\text{CoFe}_2\text{O}_4$  exhibits two dielectric relaxations in the frequency range of 1–10 kHz while Gd substituted  $\text{CoFe}_2\text{O}_4$  compositions exhibit only single relaxation at 1 kHz. The dielectric constant of  $\text{CoFe}_{2-x}\text{Gd}_x\text{O}_4$  is temperature independent up to 5500°C while the

dielectric constants increase with the increasing temperature for the temperature  $T > 5500^{\circ}\text{C}$ . The loss tangent reveals the typical behaviour of a change in relaxation rates in  $\text{CoFe}_{2-x}\text{Gd}_x\text{O}_4$  as reported in literature [11]. Magnetoresistance (MR) which is the change of a material's resistivity with an increasing magnetic field is a well-known phenomenon and an important magneto-transport property to probe the material's capability to control the electron transport properties in the sensor and spintronics applications. Most of the magnetoresistive devices are built upon ferromagnetic materials though non-magnetic materials also possess the magnetoresistive property. In ferromagnetic metals and alloys, MR effects in the order of 2% are usually obtained in low fields as reported in various literatures. In the recent past a change of even 99.9% in resistivity have already been discovered in the perovskite system  $\text{La}_{1-x}\text{Ca}_x\text{MnO}_3$ , which is termed as the "colossal" magnetoresistance. However, investigations on the above focused aspect of manganese doped cobalt ferrite nanoparticles have been rarely reported. We report in this paper the structural, temperature and the frequency dependent electrical properties, and the magnetoresistance of manganese doped cobalt ferrite nanoparticles, which may open up a new window in the field of sensor, actuator, switching and in dielectric applications.

## Experimental

The samples have been prepared by conventional solid state reaction route using the planetary ball milling technique. Three different series of samples  $\text{Co}_{1+x}\text{Mn}_x\text{Fe}_{2-x}\text{O}_4$  (CMF),  $\text{CoMn}_x\text{Fe}_{2-x}\text{O}_4$  (CFM) and  $\text{Co}_{1+x}\text{Mn}_x\text{Fe}_{2-x}\text{O}_4$  (CFMZ) were synthesized with  $x=0.125$  for all three series of samples. The powder of  $\text{Co}_2\text{O}_3$ ,  $\text{MnO}_2$  and  $\text{Fe}_2\text{O}_3$  were mixed in desired proportion and hand milled for 2 h before calcination. The hand mixed powders are calcined at  $550\text{ C}$  prior to ball milling for 12 h. The calcined powders of these samples have been analyzed for their structural properties and for scaling the particle size distribution using X-ray diffraction and Field Emission Scanning Electron microscopy (FESEM). The EDS spectrum was used to confirm the presence of compositional elements in each sample. The sample powders were then pelletized to disc shape and sintered at  $750\text{ C}$  for 1 h. These pellets were then used to measure the dielectric properties, dc resistance and impedance in a Waynekerr 6500B Impedance analyzer coupled to oven with the PID regulator for accurate temperature dependence analysis. AC resistivity ( $\rho_{ac}$ ) was calculated using

the conventional formula using the geometrical parameters of each sample. The temperature dependent measurements of ac magnetic permeability and permittivity were done at frequencies 100 Hz, 1 kHz, 10 kHz, 100 kHz and at 1 MHz. The dielectric loss factor  $\tan\delta$  was calculated from the measured values of real ( $\epsilon'$ ) and imaginary ( $\epsilon''$ ) parts of dielectric constant. The ac conductivity was calculated by using the formula  $\sigma_{ac} = 2\pi\epsilon_0 \epsilon' \tan\delta$  [12]. The current vs voltage (I-V) measurements were done using a conventional 4 point -probe method to analyze the magnetoresistance and field dependent dc resistivity for the sample series CFMZ system having composition  $\text{Co}_{1+x}\text{Mn}_x\text{Fe}_{2-x}\text{O}_4$ . The magnetoresistance was calculated using the formula

$$MR\% = \left( \frac{\rho_H}{\rho_0} - 1 \right) \times 100, \text{ where } \rho_0 \text{ is the calculated resistivity in}$$

absence of the magnetic field and  $\rho_H$  is the magnetoresistance in presence of the magnetic field. For the measurements of ac permittivity as a function of frequency and also temperature, the samples are clamped between the electrodes. Proper care was taken so that no entrapped air is present in between the electrodes and the material samples. For the measurements of ac permittivity as a function of temperature, the samples are clamped in a specific sample holder designed for the temperature dependent properties measurements. The temperature of the samples are accurately controlled using a PID controlled oven and a temperature controller.

## Results and Discussion

### Structural properties

**X-Ray Diffraction (XRD):** Figure 1 shows the X-Ray Diffraction (XRD) patterns of the studied samples. All three figures confirm the cubic spinel structures of the samples. The similar pattern is observed for all the three systems such as CMF, CFM and CFMZ however their Full Width Half Maximum (FWHM) values differ as determined by the software (match 3), which is listed in the list of structural parameters. The peak at  $30^{\circ}$ ,  $35^{\circ}$ ,  $37^{\circ}$ ,  $43^{\circ}$ ,  $54^{\circ}$ ,  $57^{\circ}$  and  $62^{\circ}$  corresponds to the crystal planes (220), (511), (222), (400), (422), (511) and (400) respectively. The presence of these planes in the patterns confirms the cubic spinel structure of all the samples along with residual oxide phases as reported in the literature [7]. The other prominent peaks in the patterns at  $26^{\circ}$ ,  $41^{\circ}$ ,  $49^{\circ}$  and  $64^{\circ}$  corresponds to the  $\text{Fe}_2\text{O}_3$  (hematite) phase, which may have originated from the low calcination temperature ( $550^{\circ}\text{C} < 800^{\circ}\text{C}$ ) as explained in the

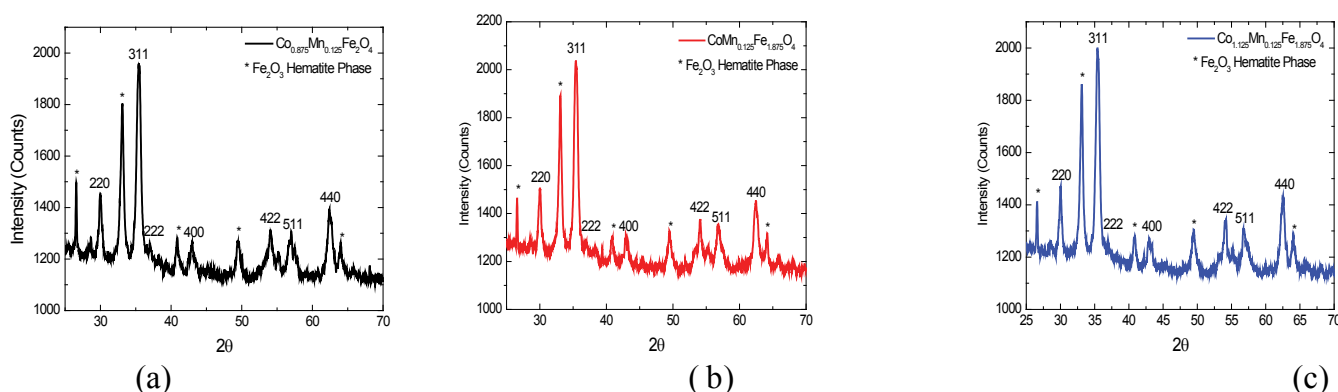


**Figure 1:** XRD Pattern for (a)  $\text{Co}_{0.875}\text{Mn}_{0.125}\text{Fe}_2\text{O}_4$  (CMF) (b)  $\text{CoMn}_{0.125}\text{Fe}_{1.875}\text{O}_4$  (CFM) and (c)  $\text{Co}_{1.125}\text{Mn}_{0.125}\text{Fe}_{1.875}\text{O}_4$  (CFMZ). *Mater Sci Nanotechnol* 2018 Volume 2 Issue 2

**Table 1: Estimated Structural parameters**

Parameters	$\text{Co}_{0.875}\text{Mn}_{0.125}\text{Fe}_2\text{O}_4$ Co/Fe = 0.44	$\text{CoMn}_{0.125}\text{Fe}_{1.875}\text{O}_4$ Co/Fe = 0.53	$\text{Co}_{1.125}\text{Mn}_{0.125}\text{Fe}_{1.875}\text{O}_4$ Co/Fe = 0.60
Crystallite size:	15.12 nm	16.71 nm	19.83 nm
Lattice Constant,	8.401 Å	8.402 Å	8.436 Å
Tetrahedral hopping length,	3.637 Å	3.638 Å	3.653 Å
Octahedra hopping length	2.970 Å	2.971 Å	2.983 Å
Tetrahedral Bond length,	1.819 Å	1.819 Å	1.827 Å
Octahedral bond length,	2.100 Å	2.100 Å	2.109 Å
X-ray density,	5.072 g/cm <sup>3</sup>	5.071 g/cm <sup>3</sup>	5.009 g/cm <sup>3</sup>
Porosity	8.989%	9.073%	8.277%
Strain	0.0075	0.0068	0.0058

literature [12]. The average crystallite size (D) of all the samples has been calculated from the corresponding highest peaks using the Scherrer’s formula [13]. The Stanley’s equations have been used to evaluate tetrahedral and octahedral hopping and bond lengths using the calculated lattice constants for all the samples. Besides the X-ray density ( $\rho_x$ ) and porosity of the samples have been calculated using  $\rho_x = \frac{\sum M}{Na^3}$  and  $p\% = 1 - \frac{\rho_x}{\rho_t}$  respectively. All the structural parameters of the studied samples are listed in the Table 1. The values of the structural parameters are in agreement with the literature values as reported in literature [7].

From Table 1 it is observed that the crystallite size, lattice constant, tetrahedral and octahedral hopping and bond lengths increase from one system to other having the same amount of Mn content (x=0.125) in the sample. The reason for increasing the aforesaid parameters is attributed to the increase in ionic radii. In the CMF system the larger  $\text{Mn}^{2+}$ (0.83 Å) replaces comparatively

smaller  $\text{Co}^{2+}$ (0.78 Å) ions whereas in CFM system it replaces further smaller  $\text{Fe}^{2+}$ (0.49 Å) ions [13] resulting in decrease in the lattice constants of CFM from CMF system. The combined effects of ionic radii of  $\text{Co}^{2+}$  and the replacement of  $\text{Fe}^{2+}$  by  $\text{Mn}^{2+}$  ions due to non-stoichiometric composition can be attributed to the increase of the aforesaid parameters in CFMZ system. The X-ray density is found to decrease and maintains the as usual inverse relationship with the lattice constant. The decreasing trend of strain can be ascribed to the increasing crystallite sizes of all the studied systems.

**Field Emission Scanning Electron Microscopy (FESEM):**

Figure 2 shows the Field Emission Scanning Electron (FESEM) micrographs along with corresponding distribution histograms of the samples of three systems namely CMF, CFM and CFMZ. The micrographs exhibit randomly agglomerated

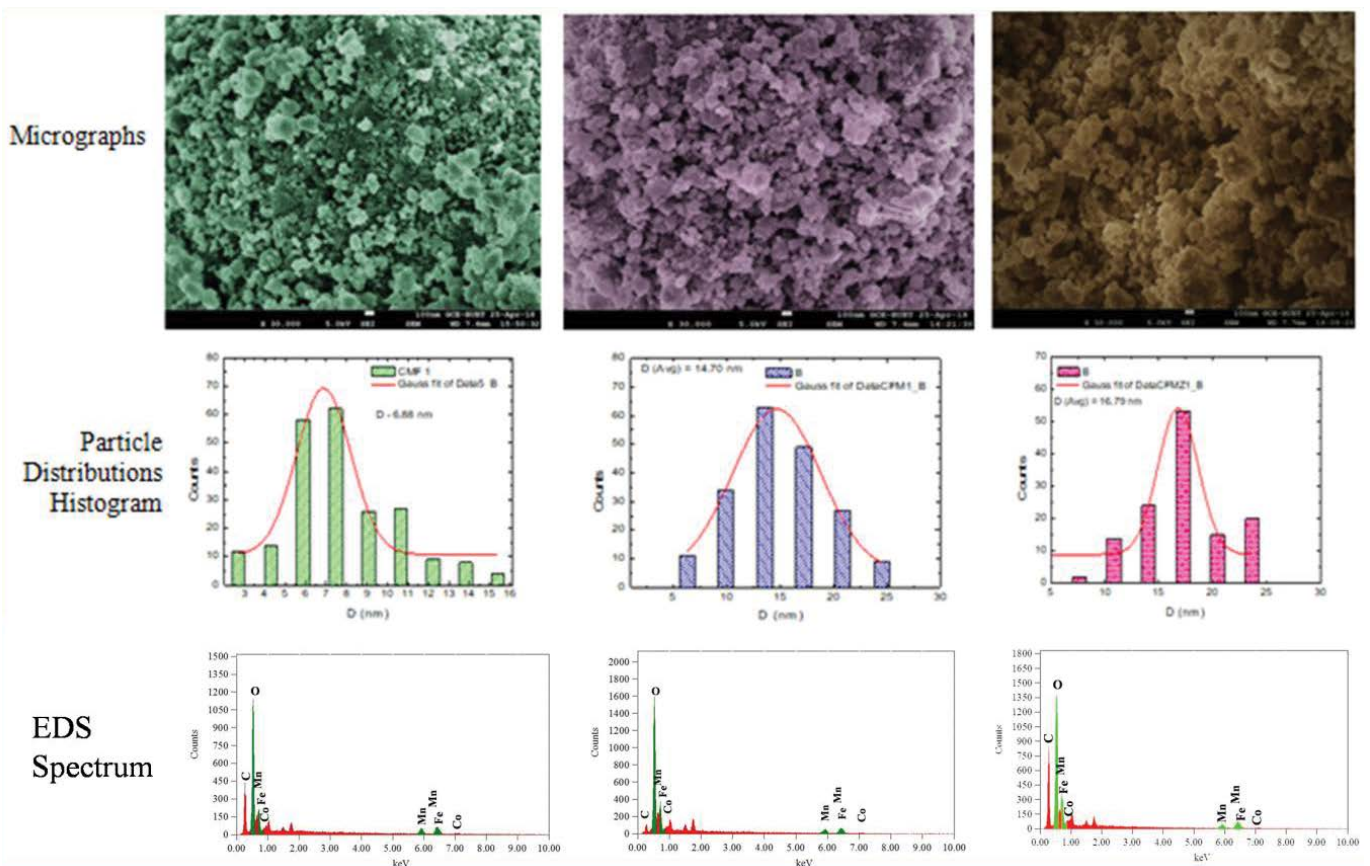


**Figure 2: FESEM micrographs, histograms and EDS spectra for  $\text{Co}_{0.875}\text{Mn}_{0.125}\text{Fe}_2\text{O}_4$  (a)  $\text{CoMn}_{0.125}\text{Fe}_{1.875}\text{O}_4$  (CFM) and (c)  $\text{Co}_{1.125}\text{Mn}_{0.125}\text{Fe}_{1.875}\text{O}_4$**

particles of nearly spherical shaped particles with average sizes 6.88 nm, 14.70 nm and 16.79 nm as estimated from the histograms of CMF, CFM and CFMZ systems respectively. It also indicates that the particle size increases as determined from the XRD patterns and is attributed to the larger ionic radii of  $\text{Co}^{2+}$  compared to  $\text{Fe}^{2+}$  ions with the increasing Co/Fe ratio (Table 1) at fixed Mn ( $x=0.125$ ) concentration. The EDS spectrum indicates the presence of Co, Mn, Fe and O in all three systems of samples. The EDS graph also indicates that the NPs are free from any impurity elements.

### Electrical properties

**Frequency dependent properties:** In an ac field, the dielectric constant becomes a complex quantity and is given by  $\epsilon = \epsilon' - j\epsilon''$  where  $\epsilon'$  is the real part which represents the stored energy, and  $\epsilon''$  is the imaginary part which corresponds to the dissipated energy [14]. The dielectric properties of ferrite materials are influenced by many factors like fabrication method, structural homogeneity, cation distribution, grain size, density, porosity, history of sintering, etc. [15,16]. Figure 3 shows the graphs for the real part ( $\epsilon'$ ), imaginary part ( $\epsilon''$ ) and the loss factor  $\tan\delta$  of dielectric constant, and ac resistivity ( $\rho_{ac}$ ) as a function of frequency at Room Temperature (RT) in logarithmic scale for the three compositions CMF, CFM and CFMZ systems while the Mn content remains constant at 0.125 (i.e.  $x=0.125$ ). Both the real part ( $\epsilon'$ ) and imaginary part ( $\epsilon''$ ) of dielectric constant as shown in Figure 3 (a) and (b) exhibit the

normal behaviour up to 0.1 MHz. This behavior of dielectric constant with the frequency can be explained on the basis of Maxwell Wagner polarization model, which states that the conductivity and dielectric properties have the common origin of charge carriers and hopping between  $\text{Fe}^{2+}$  and  $\text{Fe}^{3+}$  ions [17]. At lower frequencies, the hopping frequency of charge carriers follows the applied field, which results in the increase of the dielectric constant. However at higher frequencies, the hopping frequency of charge carriers lags behind the applied field and hence the dielectric constant decreases due to the random dipolar orientations [18]. The dispersion of  $\epsilon'$  as shown in Figure 3 (a) between 1 MHz and 10 MHz demonstrates anomalous behavior because of the change of space charge polarization to ionic polarization across the grain boundaries due to the presence of ferrous ions in the B site as explained in the literature [7]. The peak at 1 MHz in the dispersion of  $\epsilon''$  as shown in Figure 3 (b) indicates the resonance condition which implies the faster electron hopping between ferric and ferrous ions in the B site. The variation of  $\tan\delta$  with the increase of frequency as shown in Figure 3 (c) demonstrates the anomalous dielectric behavior for all the systems because of the dielectric relaxation peaks. This behavior can be explained by Rezlescu model, which states that the relaxation peaks may be produced due to collected contribution of p-type ( $\text{Co}^{2+}$ ) and n-type ( $\text{Fe}^{2+}$ ) charge carriers and small polarons, originated from the large coupling constant and narrow conduction band [17]. The pronounced leftward shift of relaxation peaks in the dispersion of  $\tan\delta$  as shown in Figures

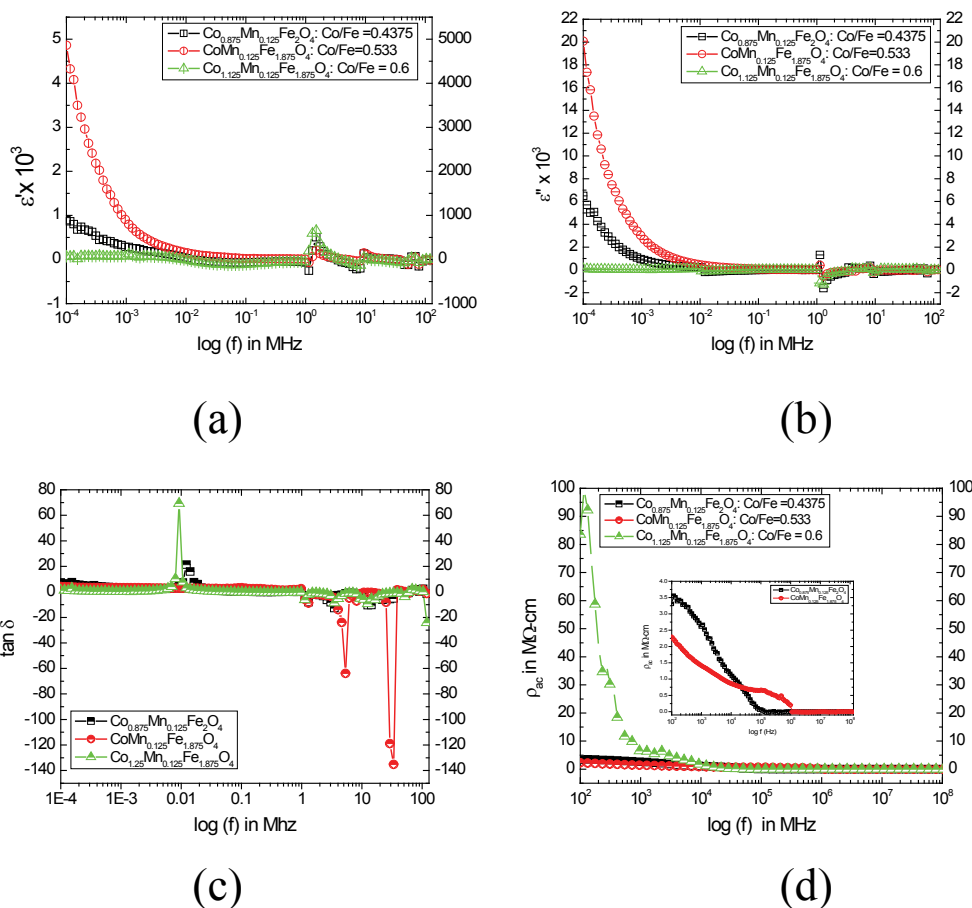


Figure 3: Graphs for (a) Real part,  $\epsilon'$ , (b) Imaginary part,  $\epsilon''$ , (c)  $\tan\delta$  loss of dielectric constant (d) ac resistivity ( $\rho_{ac}$ ) as a function of frequency.

3 (c) is observed while the Co/Fe ratio is 0.6, which may arise from the larger concentration of p-type ( $\text{Co}^{2+}$ ) carriers in the B site due to their slower mobility [5, 7]. From the Figure 3 (d) the ac resistivity ( $\rho_{ac}$ ) is found to decrease with frequency almost exponentially for all the systems. This behavior of  $\rho_{ac}$  for NPs can also be explained on the basis of Maxwell-Wagner interfacial polarization and is in agreement with Koop's phenomenological theory [19, 20], which suggested that the ferrite compact acts as multilayer capacitors and also the grain and grain boundaries have accounted for possessing different properties. The effect of multilayer capacitors increases with the increase of frequency leading to cause this decrease in  $\rho_{ac}$  as explained in the literature [18]. At low frequency i.e. below 0.001 MHz,  $\rho_{ac}$  is found to be significantly higher for the CFMZ system compared to other two systems. This behaviour is attributed to the higher Co/Fe ratio arising from the replacement of  $\text{Fe}^{2+}$  by  $\text{Mn}^{2+}$  in the B site. The ac resistivity of CMF system is found to be higher compared to that of CFMZ system below the frequency 0.01 MHz due to slower mobility of  $\text{Co}^{2+}$  (p type carriers) ions in the B site. However, above frequency 0.01, the difference in  $\rho_{ac}$  is negligibly low for all the systems and finally become constant and leading it to be independent of frequency.

**Temperature dependent properties:** The temperature dependence of dielectric constant at selected frequencies is illustrated in Figure 2 for the CFMZ system while  $x=0.125$  in the temperature range  $40^\circ\text{C} - 120^\circ\text{C}$ . At lower temperature, both the real ( $\epsilon'$ ) and imaginary ( $\epsilon''$ ) parts of dielectric constant are

found to increase for the frequencies 100 Hz, 1 kHz and 10 kHz but it is almost independent at 100 kHz and 1 MHz as seen from Figures 4 (a) and (b). At higher temperature both of them are found to decrease from different peak (temperature) points at 100 Hz, 1 kHz and 10 kHz. This nature of variation of dielectric constant is contrary to the previous results of indium substituted cobalt ferrite as reported in literature [21] and therefore unique and significant. At low but above room temperature, the initial increase of dielectric constant is likely to be originated from the additional contributions of interfacial and dipolar polarization, strongly temperature dependent, due to larger concentration of p-type ( $\text{Co}^{2+}$ ) carriers in the B site because of non-stoichiometric composition. At higher temperature, the thermal energy, supplied by the temperature boosts the mobility of charge carriers that enhances the hopping rate between A and B site and causing to reduce the interfacial polarization across the grain boundary. This phenomenon decreases the dielectric constant at higher temperature. The constancy in dielectric constant for the frequencies 100 kHz and 1 MHz is due to only presence of ionic and electronic mechanisms of polarization, which are completely independent of temperature. The decrease of dielectric constant with frequency can be ascribed to the four mechanisms of polarization. At higher frequency, only electronic contribution is present in dielectric constant whereas at lower frequencies other three mechanisms contribute to the rapid increase of dielectric constant as explained in literature [7, 14].

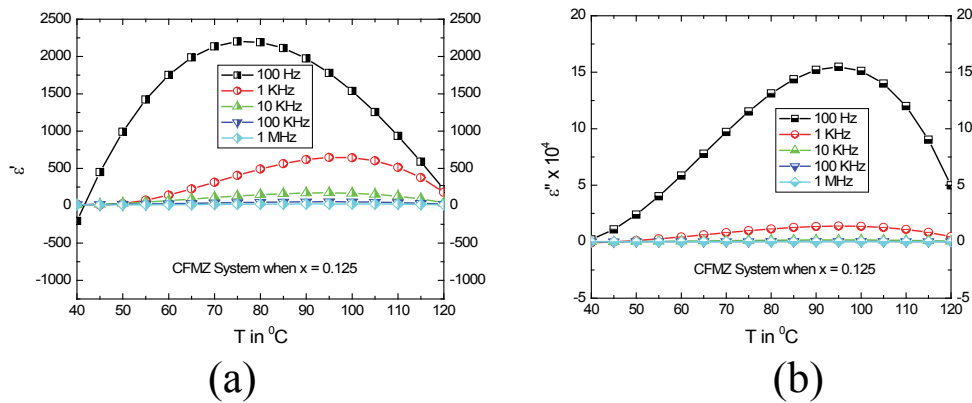


Figure 4: Graphs for (a) Real part,  $\epsilon'$  and (b) Imaginary part,  $\epsilon''$  of dielectric constant as a function of temperature of CFMZ with Mn = 0.125.

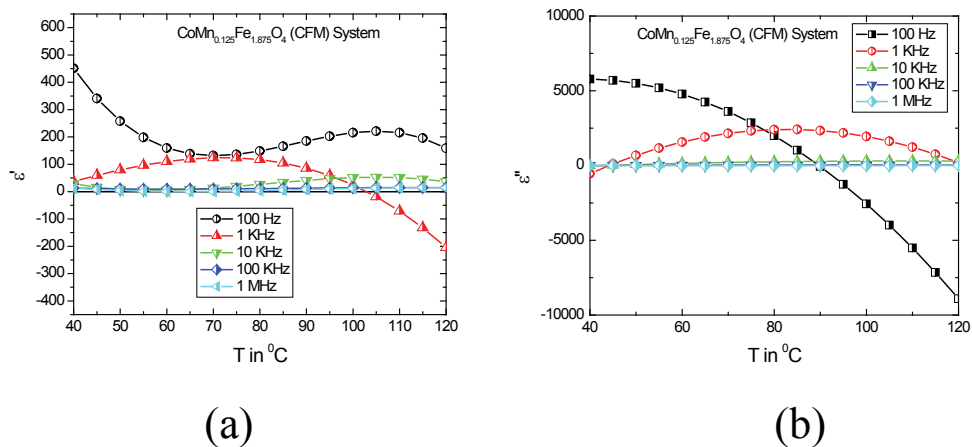


Figure 5: Graphs for (a) Real part,  $\epsilon'$  and (b) Imaginary part,  $\epsilon''$  of dielectric constant as a function of temperature of CFM with Mn = 0.125.

Figure 5 shows the variation of dielectric constant as a function of temperature (40<sup>o</sup> – 120<sup>o</sup>C) of the CFM system where x=0.125 for selective frequencies as mentioned above. The temperature dependence of dielectric constant at 100 kHz and 1 MHz is found to be similar in nature to that of the CFMZ system for the same reason as explained above. However, the variation in dielectric constant with temperature at 100 Hz is found to be dissimilar to that of CFMZ system and previously reported results of indium substituted cobalt ferrite [14]. The decreasing trend of dielectric constant at 100 Hz may be a result of transformation of interfacial polarization to ionic polarization due to hopping of charges between Co<sup>2+</sup> and Fe<sup>2+</sup> ions in the B site at the lower temperature. At higher temperature, the increase in dielectric constant is expected to be originated from the enhanced hopping rate resulted from the boosted mobility of charge carriers by the extra thermal energy from the higher temperature as explained in the case of indium substituted cobalt ferrite as reported in the literature [14]. But the variation of dielectric constant at 1 kHz is found to be similar to that of CFMZ system up to 100<sup>o</sup>C, afterwards it exhibits anomalous behavior. From Figure 5 (b), it is observed that the nature of variation of ε'' is almost similar to that of ε' up to 90<sup>o</sup>C at 100 Hz, but its negative region implies the change of polarization direction due to increase of Co<sup>2+</sup>/Fe<sup>2+</sup> ratio for the substitution of Mn<sup>2+</sup> in the B site. The increase in dielectric constant at 10 kHz and 1 MHz as seen from Figures 5 (a) and (b) is expected to cause from the only presence of electronic polarization, which is independent of temperature. The relaxation time (τ) was calculated from the peaks of ε' of dielectric constant from ε' vs.T curves as shown in Figures 4 (a) (CFMZ) and 5 (a) (CFM) using the values of ε'' of dielectric constant at corresponding temperature from ε'' vs.T curves as shown in Figures 4 (b) (CFMZ) and 5 (b) (CFM) at selected frequencies by the equation ωε'' τ = ε'(ω), modified from the Debye formula [22] since ε'∞~0 and listed in Table 2:

From Table 2, it is seen that for both the system, the relaxation time (τ) decreases with the increase of frequency, which is normal and further confirmation of dielectric behavior of the systems.

Figure 6 shows the ac resistivity (ρ<sub>ac</sub>) of both the CFM and CFMZ systems with Mn content(x=0.125) at selected frequencies in the temperature range 40<sup>o</sup>C–120<sup>o</sup> C. The ac resistivity (ρ<sub>ac</sub>) is found to decrease with the increase of temperature at all the selected frequencies for CFM system as shown in Figure 4 (a) and at selected frequencies 100 Hz, 1 kHz and 10 kHz for CFMZ system as shown in Figure 6 (b). This decrease of ρ<sub>ac</sub> exhibits the semiconductor behavior whereas the same of CFMZ system is found to increase with temperature at 100 kHz and 1 MHz as shown in Figure 6 (c), which implies the insulator behavior and displaying a signature of second order phase transition from ferri- to para- phase. The decrease in ρ<sub>ac</sub> with temperature as usually can be attributed to the thermally activated increased mobility of charge carriers that results in more transfer of electrons from one ion to another as explained in literature [14]. However the increase in ρ<sub>ac</sub> with temperature for CFMZ system at 100 kHz and 1 MHz is expected to cause from the slower mobility of greater concentration of Co<sup>2+</sup> ions (p-type carriers) in the B site due to its non-stoichiometry. These p-type carriers could not follow the ac field variation at higher frequencies (100 kHz and 1 MHz) and ultimately results in Warburg impedance in the grain boundaries due to accumulation of charge carriers across the grain boundaries. These accumulated charge carriers prohibit the charge transportation by hopping mechanism and thus causes the increase of ρ<sub>ac</sub>.

Figure 7 shows the variation of ac conductivity (σ<sub>ac</sub>) as a function of temperature of both the CMF and CFMZ systems in the temperature range 40<sup>o</sup>C–120<sup>o</sup>C at selected frequencies. It is known that the ac conductivity of dielectric materials is the summation of two terms and related by the equation σ<sub>ac</sub> = σ<sub>0</sub>(T) + σ(ω,T), where the first term σ<sub>0</sub>(T) corresponds to the dc component i.e. independent of frequency, which is related to the drifting of charge carriers and follows the Arrhenius relation but the second term σ(ω,T) is frequency dependent and related to the dielectric relaxation caused by the localized electric charge carriers. The nature of variation of σ<sub>ac</sub> with temperature for the CFM system at all selected frequencies as shown in Figure 7 (a) is almost exponential and similar to that of indium doped

Table 2: Relaxation time constant (τ)

System/Frequency	100 Hz	1 KHz	10 KHz	100 KHz	1 MHz
CFMZ System : Co <sub>1.125</sub> Mn <sub>0.125</sub> Fe <sub>1.875</sub> O <sub>4</sub>	30.28 μs	6.70 μs	1.74 μs	0.47 μs	0.19 μs
CFM System : CoMn <sub>0.125</sub> Fe <sub>1.875</sub> O <sub>4</sub>	123.57 μs	8.52 μs	2.01 μs	0.08 μs	0.01 μs

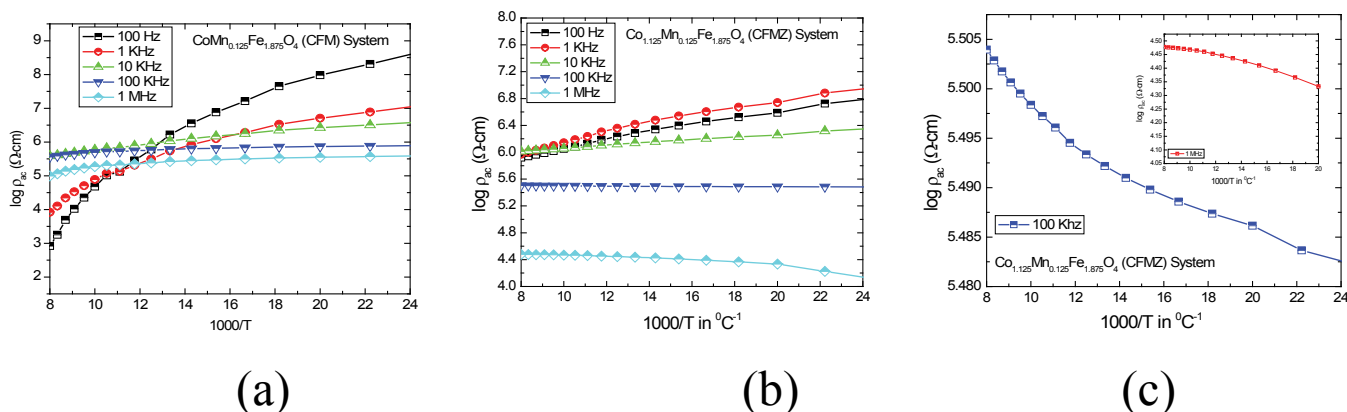


Figure 6: log(ρ<sub>ac</sub>) vs. 1000/T graphs of (a) CFM system and (b) CFMZ system for Mn content (x = 0.125) (c) CFMZ system at 100 kHz and 1 MHz. Mater Sci Nanotechnol 2018 Volume 2 Issue 2

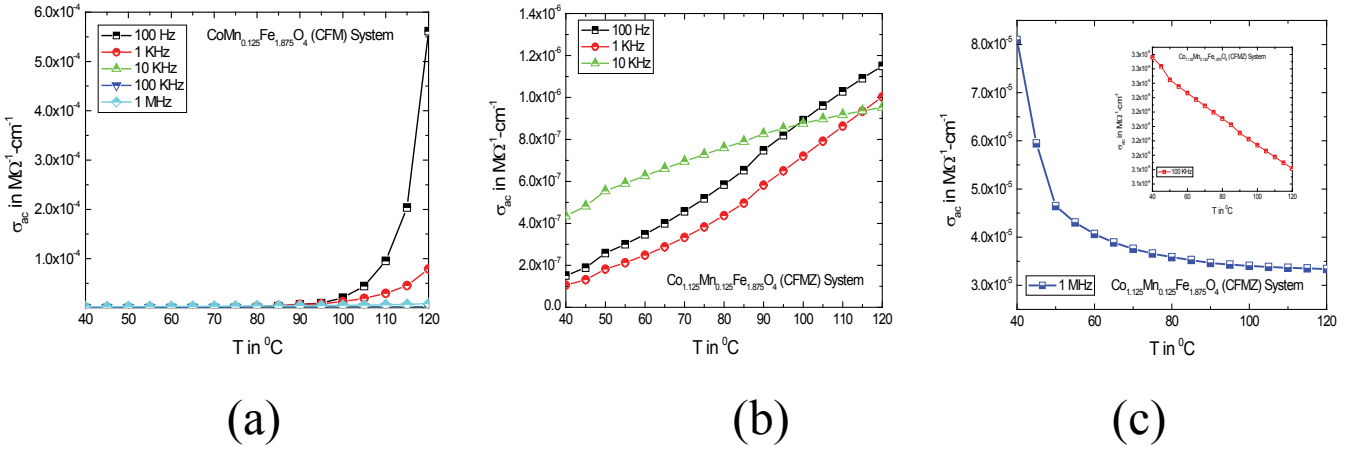


Figure 7:  $\sigma_{ac}$  vs.  $T$  graphs of (a) CFM system and (b) CFMZ system at 100 Hz, 1 kHz and 10 kHz (c) CFMZ system at 100 kHz and 1 MHz.

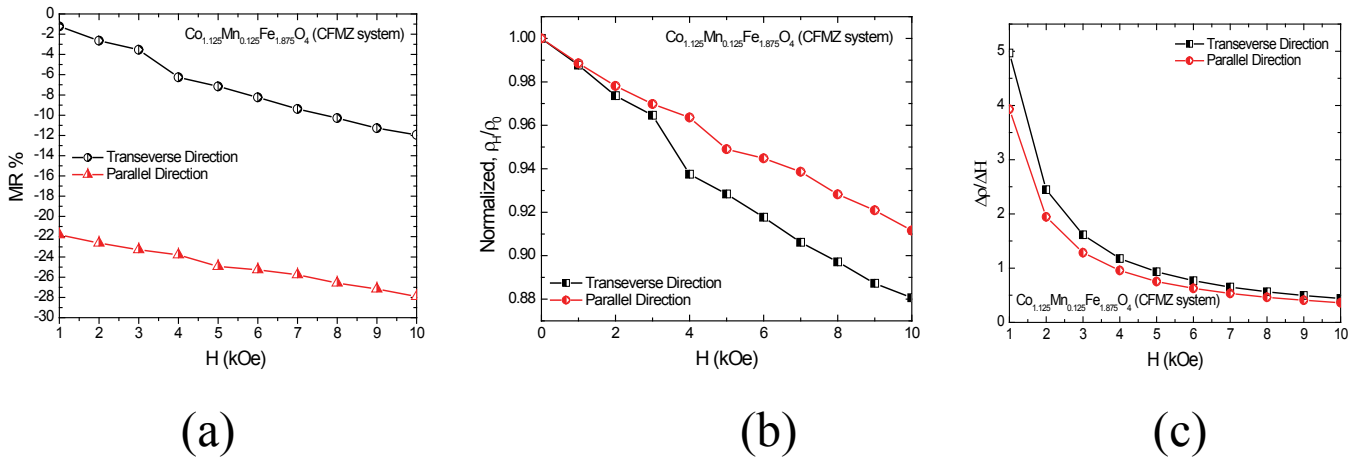


Figure 8: Graphs (a) Magnetoresistance (MR %) (b) Normalized resistivity ( $\rho_H/\rho_0$ ) as a function of magnetic field for CFMZ system with  $Mn(x) = 0.125$  (c) combined effects of the faster hopping of  $Fe^{2+}$  ions (n-type carriers) across the grain boundaries and the higher mobility of n-type carriers

cobalt ferrite nanoparticles as reported in the literature [14], which may be ascribed to the enhanced hopping of charges due to the increased mobility of charge carriers across the grain boundaries. The variation of  $\sigma_{ac}$  for the CFMZ system is almost linear with temperature at 100 Hz, 1 kHz and 10 kHz as shown in Figure 7 (b), which is significant but not in consistent with the previous reported results [17]. This nature of variation in  $\sigma_{ac}$  may be attributed to the concurrent contribution of both the n-type ( $Fe^{2+}/Fe^{3+}$ ) and p-type ( $Co^{2+}/Co^{3+}$ ) charge carriers accumulated across the grain boundaries in their hopping mechanism for ionic redistribution by thermal agitation due to its non-stoichiometry. The decrease in  $\sigma_{ac}$  with temperature is noticed at 100 kHz and 1 MHz as shown in Figure 7 (c), which corresponds to the increase in  $\rho_{ac}$ . The reason of this nature of variation in  $\sigma_{ac}$  is similar to the increase in  $\rho_{ac}$  as discussed above.

**Magnetoresistance**

Figure 8 shows the nature of variation of magnetoresistance (MR), normalized resistivity ( $\frac{\rho_H}{\rho_0}$ ) and the rate of change of resistivity ( $\frac{\Delta\rho}{\Delta H}$ ) as a function of magnetic field (H) of CFMZ system for transverse and parallel field direction to the current respectively at RT. In both the direction, negative MR is obtained and found to increase with the increase of magnetic field as shown in Figure 8 (a). This nature of variation in MR is

found to exhibit the normal behaviour and almost in agreement with the previous reported results of this kind of materials. The negative value of MR entails the dominance of n-type carriers i.e.  $Fe^{2+}$  ions in the hopping process of this system. This fact is confirmed from the decrease of normalized resistivity with the increase of magnetic field as show in Figure 8 (b), which may be ascribed to the weakening of spin-orbit coupling under the influence of externally applied magnetic field. However, the observed large value of negative MR, compared to other such ferromagnetic materials is expected to arise from the spin-dependent electron scattering due to the field induced change of the canting angle of manganese spins for inherent antiferromagnetic effect of  $Mn^{2+}$  in the B site [23]. Besides, the marked difference in MR is observed between the transverse and parallel directions to the current, which can be explained on the basis of cross section for scattering in the ferromagnetic materials. If the field and magnetization are oriented transverse to the current, then the electronic orbits are in the plane of the current, and there is a small cross-section for scattering, giving a low resistance state. Conversely for fields applied parallel to the current, the electronic orbits are oriented perpendicular to the current, and the cross-section for scattering is increased, giving a high resistance state [24]. Furthermore, the rate of change of resistivity is found to decrease almost exponentially with the

increase of the applied magnetic field as shown in Figure 8 (c) that is expected to cause from the combined effects of the faster hopping of  $\text{Fe}^{2+}$  ions (n-type carriers) across the grain boundaries and the higher mobility of n-type carriers. The higher rate of change of resistivity in the low field region may make this CFMZ system more suitable to be used in the field of position sensor and biosensor applications.

## Conclusion

Nanoparticles of three systems, CMF, CFM and CFMZ with  $\text{Mn}=0.125$  of manganese doped cobalt ferrite nanoparticles have been synthesized *via* standard solid state reaction route using the planetary ball milling technique. The existence of peaks in the XRD patterns of the 3 systems of samples confirms the formation of spinel structure. The dielectric constants show interesting relaxation behavior over certain frequency band which could be attributed to the influence of an antiferromagnetic dopant in a ferri-magnetic solute. The other measured parameters e.g., the Resistance (R) and Impedance (Z) also support the dielectric relaxation behavior of the samples in the frequency range 100 Hz to 120 MHz and temperature range  $40^{\circ}\text{C}$ – $120^{\circ}\text{C}$ . The increase of lattice constant from one compositional system to the other system with Mn content 0.125 is observed due to the effect of larger ionic radii. The average particle size is estimated to be 6.88 nm, 14.70 nm and 16.79 nm for CMF, CFM and CFMZ systems respectively from FESEM. The EDS spectrum confirms the existence of constituents with no traceable impurities. The variation of  $\tan\delta$  with the increasing frequency demonstrates the anomalous dielectric behavior for all the systems because of the dielectric relaxation peaks. This behaviour expected to be originated from the collective contributions from p-type and n-type charge carriers along with small polarons due to large coupling constant and narrow conduction band. The pronounced leftward shift of relaxation frequency in the dispersion of  $\tan\delta$  is attributed to the larger concentration of p-type ( $\text{Co}^{2+}$ ) carriers in the B site due to their slower mobility. The relaxation peaks in the dispersion of  $\tan\delta$  corresponds to the dissipation of energy and released as heat, which may be used in dielectric heating applications. At lower frequency i.e. below 1 kHz, the ac resistivity ( $\rho_{ac}$ ) is found to be significantly higher for the CFMZ system compared to other two (CFM and CMF) systems. This behavior is attributed to the higher Co/Fe due to the replacement of  $\text{Fe}^{2+}$  by  $\text{Mn}^{2+}$  in the B site. At higher temperature both the real ( $\epsilon'$ ) and imaginary ( $\epsilon''$ ) parts of dielectric constant of CFMZ system is found to decrease from different peak (temperature) points at the selected frequencies 100 Hz, 1 kHz and 10 kHz, which is unique in this case and is assumed to be the signature of ferri- to para- phase transition. The relaxation time constant ( $\tau$ ) is found to be maximum at 100 Hz and minimum at 1 MHz for CFM system as compared to that of CFMZ system from Table 1. The decreasing trend of  $\tau$  with frequency is typical of frequency dependent dielectric behavior of the studied systems. Both the system exhibits semiconductor behaviour at the selected frequencies 100 Hz, 1 kHz and 10 kHz but show insulator behavior at higher frequency regime 100 kHz-1 MHz. Materials with this kind of frequency response are suitable for switching and actuator applications. Also, the higher rate of

change of resistivity in the lower field region which is thought to have originated from the combined effects of faster hopping of  $\text{Fe}^{2+}$  ions and their higher mobility might make the CFMZ system suitable for position sensor and biosensor applications.

## Acknowledgement

The authors are thankful to the International Science Programs (ISP), Uppsala University, Sweden for financial and technical support. The authors are also thankful to the Department of Glass and Ceramics Engineering (GCE), Bangladesh University of Engineering and Technology (BUET), and to the Department of Physics, Military Institute of Science and Technology (MIST) for their experimental support.

## References

1. Waje SB, Hashim M, Ismail I. Effects of sintering temperature on grain growth and the complex permeability of  $\text{Co}_{0.2}\text{Ni}_{0.3}\text{Zn}_{0.5}\text{Fe}_2\text{O}_4$  material prepared using mechanically alloyed nanoparticles. *J Magn Magn Mater.* 2011;323(11):1433-9.
2. Ahmed R, Gul IH, Zarar M, et al. Improved Electrical Properties of Cadmium Substituted Cobalt Ferrites Nanoparticles for Microwave Application. *J Magn Magn Mater.* 2016;405:28-35.
3. Kolekar YD, Sanchez L, Rubio EJ, et al. Grain and grain boundary effects on the frequency and temperature dependent dielectric properties of cobalt ferrite-hafnium composites. *Solid State Commun.* 2014;184:34-9.
4. Shivakumar N, Narayanasamy A, Chinnasamy CN, et al. Influence of thermal annealing on the dielectric properties and electrical relaxation behaviour in nanostructured  $\text{CoFe}_2\text{O}_4$  ferrite. *J Phys Condens Matter.* 2007;19:386201.
5. Ponpandian N, Balaya P, Narayanasamy A. Electrical conductivity and dielectric behaviour of nanocrystalline  $\text{NiFe}_2\text{O}_4$  spinel. *J Phys Condens Matter.* 2002;14:3221–37.
6. Singh JP, Kumar H, Singhal A, et al. Solubility limit, magnetic interaction and conduction mechanism in rare earth doped spinel ferrite. *Applied Science Letters.* 2016;2(1):03-11.
7. Ahsan MZ, Khan FA. Study of Structural, Electrical and Magnetic Properties of Manganese Doped Cobalt Ferrite Nanoparticles with Non-stoichiometric Composition. *Journal of Physical Science and Application.* 2017;7(6):30-7.
8. Verwey EJW, Boer JH. Surface oxide films. *Journal of the Royal Netherlands Chemical Society* 1936;55(8):675-87.
9. Ugendar K, Vaithyanathan V, Patro LN, et al. Temperature-dependent magnetization, anisotropy and conductivity of  $\text{CoFe}_{2-x}\text{Sn}_x\text{O}_4$  ( $x = 0.025, 0.05, 0.075$ ): appearance of grain boundary conductivity at high temperatures. *J Phys D Appl Phys.* 2016;49:305001.
10. Khan A, Alam M, Al-Quaderi GD, et al. Dielectric and Transport Properties of Zn-Substituted Cobalt Ferrites. *J Bangladesh Acad Sci.* 2013;37(1):73-82.
11. Rahman MT, Vargas M, Ramana CV. Structural



- characteristics, electrical conduction and dielectric properties of gadolinium substituted cobalt ferrite. *J Alloy compd.* 2014;617:547–62.
12. Yadav RS, Kuřitka I, Vilcakova J, et al. Impact of grain size and structural changes on magnetic, dielectric, electrical, impedance and modulus spectroscopic characteristics of  $\text{CoFe}_2\text{O}_4$  nanoparticles synthesized by honey mediated solgel combustion method. *Advances in Natural Sciences: Nanoscience and Nanotechnology.* 2017;8:045002.
  13. Yadav SP, Shinde SS, Kadam AA, et al. Structural, morphological, dielectrical and magnetic properties of Mn substituted cobalt ferrite. *Journal of Semiconductor.* 2013;34:093002.
  14. Nongjai R, Khan S, Asokan K, et al. Magnetic and electrical properties of In doped cobalt ferrite nanoparticles. *J Appl Phys.* 2012;112:084321.
  15. Shirsath SE, Toksha BG, Jadhav KM. Structural and magnetic properties of  $\text{In}^{3+}$  substituted  $\text{NiFe}_2\text{O}_4$ . *Mater Chem Phys.* 2009;117:163.
  16. George M, Nair SS, John AM, et al. Structural, magnetic and electrical properties of the sol-gel prepared  $\text{Li}_{0.5}\text{Fe}_{2.5}\text{O}_4$  fine particles. *J Phys D Appl Phys.* 2006;39:900.
  17. Kambale RC, Shaikh PA, Bhosale CH, et al. The effect of Mn substitution on the magnetic and dielectric properties of cobalt ferrite synthesized by an auto combustion route. *Smart Mater Struct.* 2009;18:115028.
  18. Jonker GH. Analysis of the semiconducting properties of cobalt ferrite. *J Phys Chem Solids.* 1959;9:165.
  19. Rezlescu N, Rezlescu E. Dielectric properties of copper containing ferrites. *Phys Status Solidi A.* 1974;23(2):575.
  20. Koop's CG. On the Dispersion of Resistivity and Dielectric Constant of Some Semiconductors at Audio frequencies. *Phys Rev.* 1951;83(1):121–4.
  21. Nlebedim IC, Melikhov Y, Jiles DC. Temperature dependence of magnetic properties of heat treated cobalt ferrite *J Appl Phys.* 2014;15:043903.
  22. Maxwell JC. *Electricity and Magnetism.* Oxford University Press, UK. 1973.
  23. Chahara K, Ohno T, Kasai M. Magnetoresistance in magnetic manganese oxide with intrinsic antiferromagnetic spin structure. *Applied Physics Letter.* 1993;63:1990.
  24. Nickel J. *Magnetoresistance Overview.* Computer Peripherals Laboratory HPL-95-60. 1995.

**\*Correspondence to:**

F. A. Khan  
 Department of physics, Bangladesh University  
 of Engineering and Technology (BUET), Dhaka,  
 Bangladesh  
 E-mail - fakhan@phy.buet.ac.bd